

1      **Remote entanglement via adiabatic passage using a tunably-dissipative quantum**  
2      **communication system**

3      H.-S. Chang,<sup>1</sup> Y. P. Zhong,<sup>1</sup> A. Bienfait,<sup>1,\*</sup> M.-H. Chou,<sup>1,2</sup> C. R. Conner,<sup>1</sup> É. Dumur,<sup>1,3,†</sup>  
4      J. Grebel,<sup>1</sup> G. A. Pears,<sup>4,1</sup> R. G. Povey,<sup>1,2</sup> K. J. Satzinger,<sup>4,1,‡</sup> and A. N. Cleland<sup>1,3</sup>

5      <sup>1</sup>*Pritzker School of Molecular Engineering, University of Chicago, Chicago IL 60637, USA*

6      <sup>2</sup>*Department of Physics, University of Chicago, Chicago IL 60637, USA*

7      <sup>3</sup>*Argonne National Laboratory, Argonne IL 60439, USA*

8      <sup>4</sup>*Department of Physics, University of California, Santa Barbara CA 93106, USA*

9      (Dated: May 22, 2020)

10     Effective quantum communication between remote quantum nodes requires high fidelity quantum  
11    state transfer and remote entanglement generation. Recent experiments have demonstrated that  
12    microwave photons, as well as phonons, can be used to couple superconducting qubits, with a  
13    fidelity limited primarily by loss in the communication channel [1–6]. Adiabatic protocols can  
14    overcome channel loss by transferring quantum states without populating the lossy communication  
15    channel. Here we present a unique superconducting quantum communication system, comprising  
16    two superconducting qubits connected by a 0.73 m-long communication channel. Significantly,  
17    we can introduce large tunable loss to the channel, allowing exploration of different entanglement  
18    protocols in the presence of dissipation. When set for minimum loss in the channel, we demonstrate  
19    an adiabatic quantum state transfer protocol that achieves 99% transfer efficiency as well as the  
20    deterministic generation of entangled Bell states with a fidelity of 96%, all without populating  
21    the intervening communication channel, and competitive with a qubit-resonant mode-qubit relay  
22    method. We also explore the performance of the adiabatic protocol in the presence of significant  
23    channel loss, and show that the adiabatic protocol protects against loss in the channel, achieving  
24    higher state transfer and entanglement fidelities than the relay method.

25     Remote entanglement of superconducting qubits has recently been demonstrated using both microwave photon-  
26    and phonon-mediated communication [1–6]. Many of these demonstrations are limited by loss in the communication  
27    channel, due to loss in the various microwave components or intrinsic to the channel itself [1, 4, 6]; similar limitations  
28    apply to e.g. optically-based quantum communication systems. Adiabatic protocols analogous to stimulated Raman  
29    adiabatic passage (STIRAP) [7, 8] can mitigate such loss by adiabatically evolving an eigenstate of the system, using  
30    states that are “dark” with respect to the communication channel. These enable the high-fidelity coherent transfer  
31    of quantum states between sender and receiver nodes, even in the presence of large channel loss. Despite their use in  
32    a number of localized systems, such protocols have not been used for the generation of remote entangled states [7, 8].

33     In this Letter, we present a unique experimental system comprising a pair of superconducting transmon-style  
34    qubits linked by an on-chip, 0.73 m-long superconducting microwave transmission line. By changing the coupling of  
35    the transmission line to a resistive load, we can vary the transmission line’s energy lifetime  $T_{1r}$  over two orders of  
36    magnitude. We demonstrate an adiabatic protocol for quantum communication between the qubit nodes, compare  
37    its performance to a qubit-transmission mode-qubit relay method [5, 9, 10], and explore the performance of both

38 protocols as a function of transmission loss.

39 We first describe the experimental device, then the two-state transfer methods. We test the performance of each  
 40 protocol in the low-loss limit, then as a function of transmission loss. The adiabatic process achieves significantly  
 41 improved performance compared to the relay method, especially at intermediate levels of loss in the channel.

42 The two quantum state transfer methods, and the device we use to test them, are shown in Fig. 1. The device  
 43 comprises two frequency-tunable superconducting xmon qubits [11, 12],  $Q_1$  and  $Q_2$ , each coupled to one end of the  
 44 on-chip transmission line via an electrically-controlled tunable coupler [13],  $G_1$  and  $G_2$  respectively (Fig. 1b). We use  
 45 the qubit ground  $|g\rangle$  and excited  $|e\rangle$  states, whose transition frequency is tunable from  $\sim 3$  to 6 GHz. Qubit control is  
 46 via low-frequency flux-tuning for  $Z$  control and quadrature-resolved microwave pulses for  $XY$  control. We read out  
 47 the qubit states using standard dispersive measurements [14–16], via a capacitively-coupled readout resonator and a  
 48 traveling-wave parametric amplifier. We projectively measure the excited state probability  $P_e$  of each qubit with a  
 49 fidelity of  $88.8 \pm 0.8\%$ .

50 The tunable couplers  $G_1$  and  $G_2$  allow us to externally control the coupling  $g_{1,2}$  of each qubit to the individual  
 51 resonant modes in the transmission line. A variable control consisting of two additional tunable couplers,  $D_1$  and  
 52  $D_2$ , is integrated into the transmission line, 1.6 mm from the coupler  $G_1$  and its associated qubit  $Q_1$ . This circuit  
 53 element provides electrically-controlled coupling between its input port and two output ports [17]. The coupler  $D_2$  is  
 54 placed inline with the transmission line and is always set to provide maximum coupling (and minimal reflection) to  
 55 the remaining length of transmission line. The other coupler  $D_1$  connects to port 1 on the sample mount, which is  
 56 terminated by a lumped  $50 \Omega$  microwave load outside the sample box. Varying the coupling to this load allows us to  
 57 set the loss in the transmission line, quantified by the energy lifetime  $T_{1r}$  of each resonant mode.

58 The transmission line of length  $\ell = 0.73$  m supports multiple resonant modes, separated in frequency by the free  
 59 spectral range  $\omega_{\text{FSR}}/2\pi = 1/2T_\ell = 84$  MHz, where  $T_\ell = 5.9$  ns is the photon one-way transit time in the channel. For  
 60 sufficiently small qubit-resonator coupling,  $g_{1,2} \ll \omega_{\text{FSR}}$ , each qubit can be selectively coupled to a single resonant  
 61 mode in the transmission line. This is shown in Fig. 2a, where the transition frequency  $\omega_{ge}/2\pi$  of qubit  $Q_1$  is tuned  
 62 over 400 MHz, yielding four separate vacuum Rabi swap resonances spaced by the free spectral range  $\omega_{\text{FSR}}/2\pi$ .  
 63 The loss coupler  $D_1$  was set to minimum coupling, so the transmission line is limited only by its intrinsic loss. All  
 64 experiments here were done with the mode at 5.351 GHz, just to the right of center in Fig. 2a.

65 In Fig. 2b, we demonstrate tunable control over the channel loss, using qubit  $Q_1$  to measure the lifetime of the  
 66 resonant mode at 5.531 GHz as we vary the coupler  $D_1$  and thus the transmission line loss. The pulse sequence for  
 67 this measurement is shown inset in Fig. 2b. The mode energy decay time  $T_{1r}$  for each loss setting (controlled by  
 68 the  $D_1$  flux) is shown in Fig. 2b. With no coupling through  $D_1$ , we measure the intrinsic resonant mode lifetime  
 69  $T_{1r} \approx 3410 \pm 40$  ns (orange), comparable to similar transmission lines without variable loss [5]. With maximum  
 70 coupling to the load, we measure a lifetime  $T_{1r} \approx 28.7 \pm 0.2$  ns (blue), corresponding to a loaded quality factor  
 71  $Q_r = 960$ , about 120 times smaller than the intrinsic quality factor of  $1.1 \times 10^5$ . We also measure the resonant  
 72 mode's Ramsey dephasing time  $T_{2r}$  at various  $D_1$  flux bias points, and find  $T_{2r} \approx 2T_{1r}$ , indicating the coupler  $D_1$   
 73 introduces negligible additional phase decoherence. One non-ideality with this system is that qubit  $Q_1$ , due to its close  
 74 proximity to the loss coupler  $D_1$ , also has its lifetime reduced when the couplers  $G_1$  and  $D_1$  are both set to non-zero

75 coupling, allowing energy loss from  $Q_1$  to the external load; this limits  $Q_1$ ’s performance, and is discussed further in  
 76 the Supplementary Information [17–36]. This additional loss pathway could be reduced by placing the loss coupler  
 77  $D_1$  in the center of transmission line, as the transmission line would then protect both qubits from the external load.

78 We used two different communication protocols, adiabatic transfer and a qubit-resonant mode-qubit relay method.  
 79 Both methods were used for qubit state transfer via the transmission line as well as Bell state generation, both as a  
 80 function of loss in the communication channel. The relay method uses a single extended mode in the transmission  
 81 line, swapping an excitation from one qubit into that mode and subsequently swapping the excitation from that mode  
 82 to the other qubit. This method is described in detail elsewhere [5]; here it achieves an intrinsic loss-limited state  
 83 transfer efficiency of  $\eta = 0.95 \pm 0.01$  and a Bell state fidelity of  $\mathcal{F}_s = \langle \psi^- | \rho | \psi^- \rangle = 0.941 \pm 0.005$ , where  $\rho$  is the  
 84 measured density matrix and  $|\psi^-\rangle = (|eg\rangle - |ge\rangle)/\sqrt{2}$  is the reference Bell singlet state.

85 The adiabatic method uses the variable coupling of each qubit to the transmission line. When qubits  $Q_1$  and  $Q_2$   
 86 are set to the same frequency and couple to the same resonant mode in the channel with strengths  $g_1(t)$  and  $g_2(t)$ ,  
 87 the single-excitation Hamiltonian for the system can be written in the rotating frame as

$$H/\hbar = g_1(t) (|e0g\rangle\langle g1g| + |g1g\rangle\langle e0g|) + g_2(t) (|g0e\rangle\langle g1g| + |g1g\rangle\langle g0e|), \quad (1)$$

88 where  $|aNb\rangle$  corresponds to  $Q_1$  ( $Q_2$ ) in  $|a\rangle$  ( $|b\rangle$ ) with  $N$  photons in the resonant transmission line mode. This  
 89 Hamiltonian supports a “dark” eigenstate  $|D\rangle$  that has no occupancy in the resonant mode,

$$|D(t)\rangle = \frac{1}{\sqrt{2}} (\cos \theta(t) |e0g\rangle - \sin \theta(t) |g0e\rangle), \quad (2)$$

90 where the mixing angle  $\theta$  is given by  $\tan \theta(t) = g_1(t)/g_2(t)$ . With  $g_1$  set to zero and  $g_2$  to its maximum, the dark state  
 91 is  $|D\rangle = |e0g\rangle$ , while exchanging the coupling values  $g_1 \leftrightarrow g_2$  yields the dark state  $|g0e\rangle$ . By adiabatically varying  
 92 the ratio  $g_1(t)/g_2(t)$  in time from zero to its maximum, the system will swap the excitation from  $Q_1$  to  $Q_2$ , without  
 93 populating the lossy intermediate channel [7, 37].

94 Here, we implement a simple adiabatic scheme [37, 38], where we vary the couplings in time according to  $g_1(t) =$   
 95  $\bar{g} \sin(\pi t/2t_f)$  and  $g_2(t) = \bar{g} \cos(\pi t/2t_f)$ . We choose the parameters  $\bar{g}/2\pi = 15$  MHz and  $t_f = 132$  ns, minimizing  
 96 the impact of finite qubit coherence while maintaining sufficient adiabaticity (see [18]). We note that the adiabatic  
 97 protocol supports better than 90% transfer efficiency even when  $\bar{g} = 0.4 \omega_{\text{FSR}}$ ; see [18].

98 In Fig. 3a, we demonstrate deterministic adiabatic state transfer from  $Q_1$  to  $Q_2$ . With  $Q_1$  in  $|e\rangle$  and  $Q_1$  and  $Q_2$   
 99 set on-resonance with a single mode in the channel, we adjust the couplers  $G_1$  and  $G_2$  adiabatically to complete the  
 100 state transfer. We show the excited state population of each qubit as a function of time  $t$ , measured with the resonant  
 101 mode loss at its intrinsic minimum. We observe the expected gradual population transfer from  $Q_1$  to  $Q_2$ , with  $Q_2$ ’s  
 102 population reaching its maximum at  $t = t_f$ , with a transfer efficiency  $\eta = P_{e,Q_2}(t = t_f)/P_{e,Q_1}(t = 0) = 0.99 \pm 0.01$ .  
 103 We further characterize the state transfer by carrying out quantum process tomography [39], yielding the process  
 104 matrix  $\chi$  shown inset in Fig. 3a, with a process fidelity  $\mathcal{F}_p = 0.96 \pm 0.01$ , limited by qubit decoherence. The process  
 105 matrix calculated from a master equation simulation displays a small trace distance to the measured  $\chi$  matrix of  
 106  $\mathcal{D} = \sqrt{\text{Tr}([\chi - \chi_{\text{sim}}]^2)} = 0.02 \pm 0.01$ , indicating excellent agreement with experiment.

107 The adiabatic protocol can also be used to generate remote entanglement between  $Q_1$  and  $Q_2$ . With  $Q_1$  prepared  
 108 in  $|e\rangle$ , we share half its excitation with  $Q_2$  using the adiabatic protocol, by stopping the transfer at its midpoint

<sup>109</sup>  $t = t_f/2$ . This generates a Bell singlet state  $|\psi^-\rangle = (|eg\rangle - |ge\rangle)/\sqrt{2}$ . The qubit excited state population is shown as  
<sup>110</sup> function of time  $t$  in Fig. 3b. We further characterize the Bell state by quantum state tomography [40, 41], and the  
<sup>111</sup> reconstructed density matrix  $\rho$  is shown inset in Fig. 3b. We find a Bell state fidelity  $\mathcal{F}_s = \langle \psi^- | \rho | \psi^- \rangle = 0.964 \pm 0.007$ ,  
<sup>112</sup> referenced to the ideal Bell singlet state  $\psi^-$ , and a concurrence  $\mathcal{C} = 0.95 \pm 0.01$  (see [18]). The density matrix  $\rho_{\text{sim}}$   
<sup>113</sup> calculated from a master equation simulation shows a small trace distance to the measured  $\rho$ ,  $\sqrt{\text{Tr}(|\rho - \rho_{\text{sim}}|^2)} = 0.01$ ,  
<sup>114</sup> indicating excellent agreement with experiment.

<sup>115</sup> We explore the impact of loss on both the relay method and the adiabatic protocol, with results shown as a function  
<sup>116</sup> of the resonant channel mode energy lifetime  $T_{1r}$  in Fig 4. For the highest level of dissipation, with  $T_{1r} = 28.7$  ns, we  
<sup>117</sup> measure an adiabatic transfer efficiency  $\eta = 0.67 \pm 0.01$ , even though the transfer time  $t_f$  is four times the resonant  
<sup>118</sup> mode lifetime. The efficiency is primarily limited by loss in qubit  $Q_1$  due to its spurious coupling loss through  $D_1$   
<sup>119</sup> to the  $50 \Omega$  load (see [18]), in good agreement with master equation simulations. Results from a simulation without  
<sup>120</sup> the spurious coupling are plotted as black dashed lines in Fig 4a, limited by a small channel occupation due to the  
<sup>121</sup> finite adiabaticity of the sequence. We compare these results to the relay method, where we use a weak coupling  
<sup>122</sup>  $|g_{1,2}|/2\pi = 5.0$  MHz to ensure the qubits only couple to a single transmission line mode; this results in a total transfer  
<sup>123</sup> time  $2\tau_{\text{swap}} = 100$  ns. We find the adiabatic protocol consistently performs better than the relay method, with a  
<sup>124</sup>  $2.6 \times$  higher transfer efficiency  $\eta$  ( $2.3 \times$  reduction in transfer loss) and  $1.5 \times$  higher process fidelity  $\mathcal{F}_p$  ( $2.3 \times$  reduction  
<sup>125</sup> in process infidelity) compared to the relay method in the most dissipative case; the adiabatic protocol is primarily  
<sup>126</sup> limited by spurious coupling loss in  $Q_1$ , while the relay method is limited by loss in the channel (see [18]).

<sup>127</sup> In Fig. 4b, we display the entanglement fidelity using the adiabatic protocol with different levels of channel loss,  
<sup>128</sup> and compare to the relay method. The adiabatic protocol outperforms the relay method in all levels of dissipation.  
<sup>129</sup> At the highest loss level, where  $T_{1r} = 28.7$  ns, the adiabatic protocol achieves  $1.2 \times$  higher Bell state fidelity  $\mathcal{F}_s$  ( $1.5 \times$   
<sup>130</sup> reduction in Bell state infidelity) and  $1.3 \times$  higher concurrence  $\mathcal{C}$  ( $1.7 \times$  reduction in concurrence infidelity) compared  
<sup>131</sup> to the relay method; the spurious-coupling-free simulation result for the adiabatic protocol is shown by the black  
<sup>132</sup> dashed lines, limited by a small channel occupation due to the finite adiabaticity of the sequence.

<sup>133</sup> In conclusion, we describe a unique experimental system in which we can explore the performance of quantum  
<sup>134</sup> communication protocols in the presence of controllable communication loss. We demonstrate an adiabatic protocol  
<sup>135</sup> that realizes high-fidelity transfer of quantum states and entangled Bell states, limited mostly by spurious coupling  
<sup>136</sup> of one qubit to the controlled transmission line loss. The platform we have developed is well-suited to explore the  
<sup>137</sup> impact of channel loss on other error-protecting quantum communication protocols, such as heralding [42–44] and  
<sup>138</sup> entanglement distillation [45–47]. The ability to introduce controlled loss dynamically into the system opens the door to  
<sup>139</sup> study dissipative dynamics in non-equilibrium systems, enabling approaches such as reservoir engineering [48, 49]. The  
<sup>140</sup> adiabatic protocol demonstrated here is applicable to other quantum communication systems, for example phonon-  
<sup>141</sup> based systems where the communication channel is significantly more lossy [6, 50, 51]. Future demonstrations could  
<sup>142</sup> employ more advanced adiabatic protocols such as shortcuts to adiabaticity [52, 53] and composite adiabatic passage  
<sup>143</sup> [54, 55] to further improve fidelity.

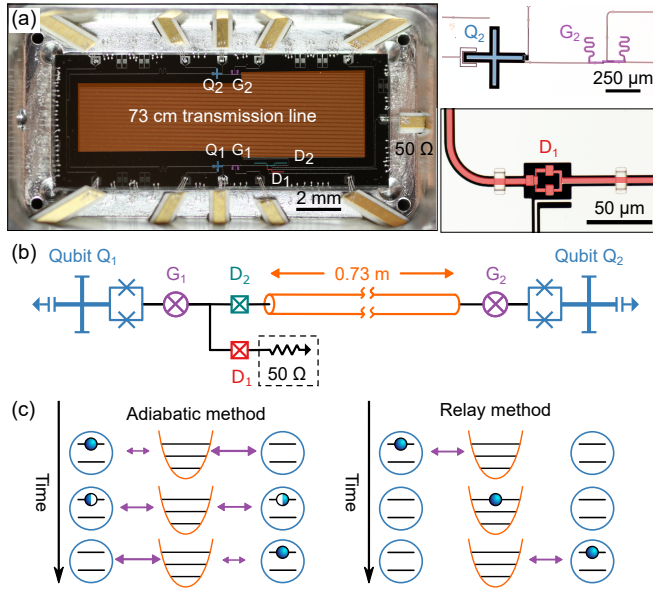


FIG. 1. Experimental device. (a) Optical micrograph of the device (left), with magnified views of one qubit and its associated tunable coupler (right top), and one variable loss coupler (right bottom). (b) A simplified circuit schematic, with two superconducting qubits ( $Q_1$  and  $Q_2$ , blue), coupled by tunable couplers ( $G_1$  and  $G_2$ , purple) to a 0.73 m-long superconducting transmission line (orange). The transmission line is interrupted near  $Q_1$  by a tunable switch. The switch comprises two tunable couplers  $D_1$  (red) and  $D_2$  (teal), with  $D_1$  connected to an external  $50\ \Omega$  load to ground (dashed box), while  $D_2$  connects to the remainder of the transmission line. Complete circuit diagram and parameters are provided in [18].

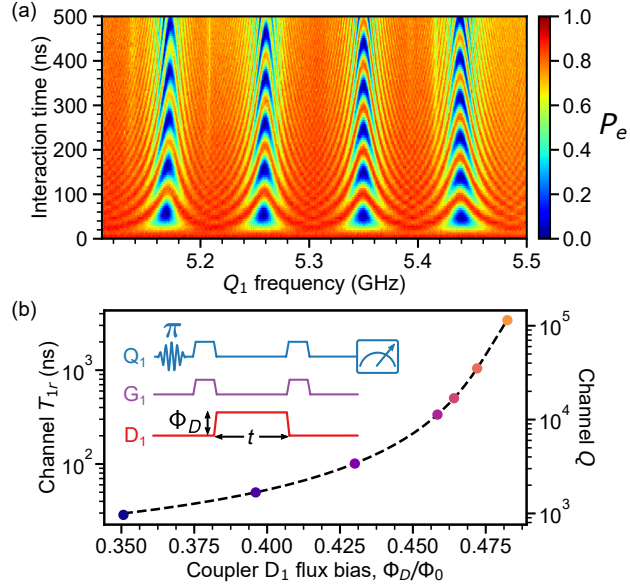


FIG. 2. Variable loss transmission channel. (a) Vacuum Rabi swaps between qubit  $Q_1$  and four sequential resonant transmission line modes. The coupling is set to  $|g_1|/2\pi = 5.0 \pm 0.1$  MHz  $\ll \omega_{\text{FSR}}/2\pi$ . (b) Measurement of the energy lifetime  $T_{1r}$  of one resonant mode in the transmission line, at 5.351 GHz, with equivalent quality factors  $Q$  shown on right; inset shows pulse sequence. A  $\pi$  pulse to qubit  $Q_1$  puts it in the excited state, and this excitation is swapped into the resonant mode for a time  $t$ , after which it is recovered and the qubit  $P_e$  measured. The corresponding lifetime is measured as a function of transmission line loss, controlled during the lifetime measurement using coupler  $D_1$ . With  $D_1$  turned off, we find the intrinsic lifetime  $T_{1r} = 3410 \pm 40$  ns (orange); with maximum loss, we find  $T_{1r} = 28.7 \pm 0.2$  ns (blue). The standard deviation of each data point is smaller than the points. Dashed lines are results calculated with a circuit model; see [18].

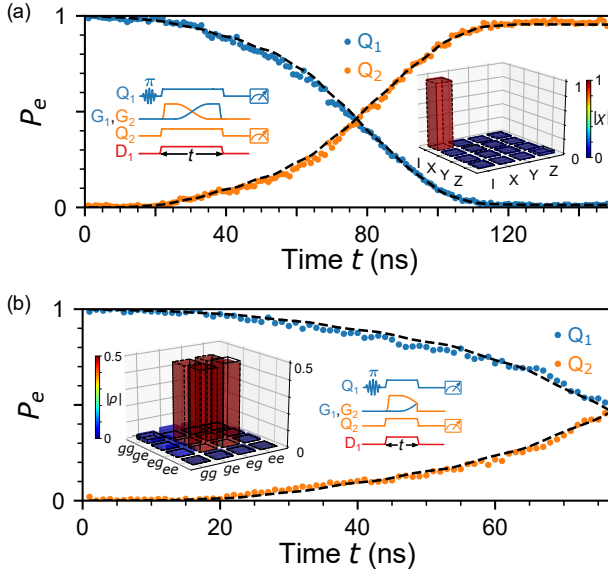


FIG. 3. Quantum state transfer and remote entanglement using the adiabatic protocol. (a) Adiabatic state transfer between qubits  $Q_1$  and  $Q_2$ , measured with intrinsic loss in the transmission line. Blue (orange) circles represent excited state populations of  $Q_1$  ( $Q_2$ ) measured simultaneously at time  $t$ . Left inset: Control pulse sequence. The couplers are set so that coupling  $g_2$  starts at its maximum with  $g_1$  set to zero. Dissipation in the resonant channel mode is controlled using  $D_1$ , here set to zero coupling. Right inset: Quantum process tomography, yielding a process fidelity  $\mathcal{F}_p = 0.96 \pm 0.01$ . (b) Adiabatic remote entanglement. Right inset shows control pulse sequence: With  $Q_1$  initially prepared in  $|e\rangle$ ,  $G_1$  and  $G_2$  are controlled using the adiabatic protocol to share half of  $Q_1$ 's excitation with  $Q_2$ , resulting in a Bell singlet state  $|\psi^-\rangle = (|eg\rangle - |ge\rangle)/\sqrt{2}$ . Blue (orange) circles represent excited state populations of  $Q_1$  ( $Q_2$ ) measured simultaneously at time  $t$ . Left inset: Reconstructed density matrix of the final Bell state, yielding a state fidelity  $\mathcal{F}_s = 0.964 \pm 0.007$  and concurrence  $\mathcal{C} = 0.95 \pm 0.01$ . In all panels, dashed lines are from master equation simulations accounting for channel dissipation and qubit imperfections (see [18]).

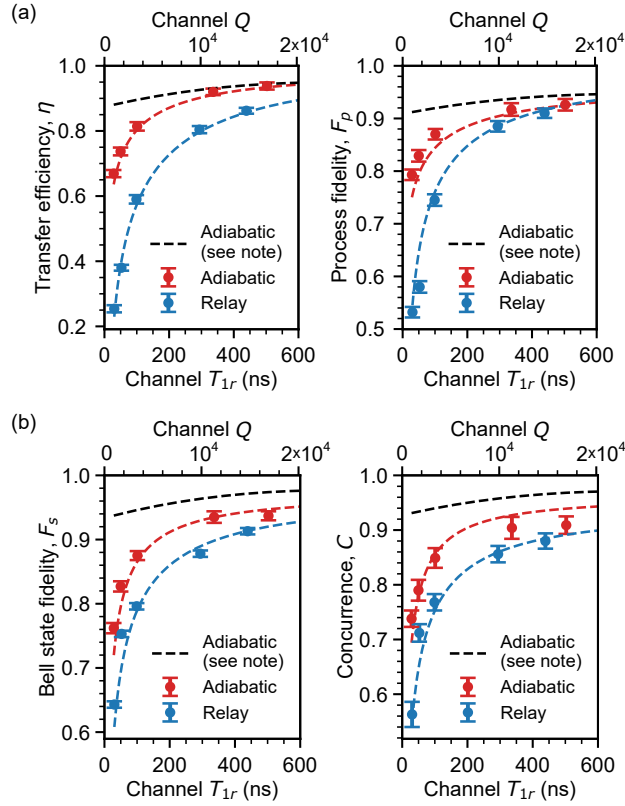


FIG. 4. Quantum communication in the presence of channel loss, using both the relay method and adiabatic protocol. (a) Measured transfer efficiency  $\eta$  (left) and process fidelity  $\mathcal{F}_p$  (right) for the adiabatic protocol (red) and the relay method (blue), for different resonant channel mode lifetimes  $T_{1r}$ , with equivalent quality factors  $Q$  shown on top. (b) Measured Bell state fidelity  $\mathcal{F}_s$  (left) and concurrence  $\mathcal{C}$  (right) for adiabatic protocol (red) and relay method (blue). In all panels, error bars are one standard deviation; red and blue dashed lines are from simulations including all sources of loss and black dashed lines are from a master equation simulation for the adiabatic protocol with no  $Q_1$  spurious coupling loss (see [18]).

144

**ACKNOWLEDGEMENTS**

145 The authors thank A. A. Clerk, P. J. Duda, and B. B. Zhou for helpful discussions. We thank W. D. Oliver and  
146 G. Calusine at MIT Lincoln Lab for providing the traveling-wave parametric amplifier (TWPA) used in this work.  
147 Devices and experiments were supported by the Air Force Office of Scientific Research and the Army Research Labo-  
148 ratory. K.J.S. was supported by NSF GRFP (NSF DGE-1144085), É.D. was supported by LDRD funds from Argonne  
149 National Laboratory; A.N.C. was supported in part by the DOE, Office of Basic Energy Sciences. This work was  
150 partially supported by the UChicago MRSEC (NSF DMR-1420709) and made use of the Pritzker Nanofabrication  
151 Facility, which receives support from SHyNE, a node of the National Science Foundation's National Nanotechnology  
152 Coordinated Infrastructure (NSF NNCI-1542205). The authors declare no competing financial interests. Correspon-  
153 dence and requests for materials should be addressed to A. N. Cleland (anc@uchicago.edu).

<sup>154</sup> \* Present address: Université de Lyon, ENS de Lyon, Université Claude Bernard, CNRS, Laboratoire de Physique, F-69342  
<sup>155</sup> Lyon, France

<sup>156</sup> † Present address: Université Grenoble Alpes, CEA, INAC-Phelip, 38000 Grenoble, France

<sup>157</sup> ‡ Present address: Google, Santa Barbara CA 93117, USA.

<sup>158</sup> [1] P. Kurpiers, P. Magnard, T. Walter, B. Royer, M. Pechal, J. Heinsoo, Y. Salathe, A. Akin, S. Storz, J.-C. Besse, S. Gasparinetti, A. Blais, and A. Wallraff, Deterministic quantum state transfer and remote entanglement using microwave photons, *Nature* **558**, 264 (2018).

<sup>161</sup> [2] C. J. Axline, L. D. Burkhardt, W. Pfaff, M. Zhang, K. Chou, P. Campagne-Ibarcq, P. Reinhold, L. Frunzio, S. M. Girvin, L. Jiang, M. H. Devoret, and R. J. Schoelkopf, On-demand quantum state transfer and entanglement between remote microwave cavity memories, *Nature Physics* **14**, 705 (2018).

<sup>164</sup> [3] P. Campagne-Ibarcq, E. Zalys-Geller, A. Narla, S. Shankar, P. Reinhold, L. Burkhardt, C. Axline, W. Pfaff, L. Frunzio, R. J. Schoelkopf, and M. H. Devoret, Deterministic remote entanglement of superconducting circuits through microwave two-photon transitions, *Physical Review Letters* **120**, 200501 (2018).

<sup>167</sup> [4] N. Leung, Y. Lu, S. Chakram, R. K. Naik, N. Earnest, R. Ma, K. Jacobs, A. N. Cleland, and D. I. Schuster, Deterministic bidirectional communication and remote entanglement generation between superconducting qubits, *npj Quantum Information* **5**, 18 (2019).

<sup>170</sup> [5] Y. P. Zhong, H.-S. Chang, K. J. Satzinger, M.-H. Chou, A. Bienfait, C. R. Conner, É. Dumur, J. Grebel, G. A. Pears, R. G. Povey, D. I. Schuster, and A. N. Cleland, Violating Bell's inequality with remotely connected superconducting qubits, *Nature Physics* **15**, 741 (2019).

<sup>173</sup> [6] A. Bienfait, K. J. Satzinger, Y. P. Zhong, H.-S. Chang, M.-H. Chou, C. R. Conner, É. Dumur, J. Grebel, G. A. Pears, R. G. Povey, and A. N. Cleland, Phonon-mediated quantum state transfer and remote qubit entanglement, *Science* **364**, 368 (2019).

<sup>176</sup> [7] N. V. Vitanov, A. A. Rangelov, B. W. Shore, and K. Bergmann, Stimulated Raman adiabatic passage in physics, chemistry, and beyond, *Reviews of Modern Physics* **89**, 015006 (2017).

<sup>178</sup> [8] K. Bergmann, H.-C. Nagerl, C. Panda, G. Gabrielse, E. Miloglyadov, M. Quack, G. Seyfang, G. Wichmann, S. Ospelkaus, A. Kuhn, S. Longhi, A. Szameit, P. Pirro, B. Hillebrands, X.-F. Zhu, J. Zhu, M. Drewsen, W. K. Hensinger, S. Weidt, T. Halfmann, H.-L. Wang, G. S. Paraoanu, N. V. Vitanov, J. Mompart, T. Busch, T. J. Barnum, D. D. Grimes, R. W. Field, M. G. Raizen, E. Narevicius, M. Auzinsh, D. Budker, A. Pálffy, and C. H. Keitel, Roadmap on STIRAP applications, *Journal of Physics B: Atomic, Molecular and Optical Physics* **52**, 202001 (2019).

<sup>183</sup> [9] M. A. Sillanpää, J. I. Park, and R. W. Simmonds, Coherent quantum state storage and transfer between two phase qubits via a resonant cavity, *Nature* **449**, 438 (2007).

<sup>185</sup> [10] M. Ansmann, H. Wang, R. C. Bialczak, M. Hofheinz, E. Lucero, M. Neeley, A. D. O'Connell, D. Sank, M. Weides, J. Wenner, A. N. Cleland, and J. M. Martinis, Violation of Bell's inequality in Josephson phase qubits, *Nature* **461**, 504 (2009).

<sup>188</sup> [11] J. Koch, T. M. Yu, J. Gambetta, A. A. Houck, D. I. Schuster, J. Majer, A. Blais, M. H. Devoret, S. M. Girvin, and R. J. Schoelkopf, Charge-insensitive qubit design derived from the Cooper pair box, *Physical Review A* **76**, 042319 (2007).

<sup>190</sup> [12] R. Barends, J. Kelly, A. Megrant, D. Sank, E. Jeffrey, Y. Chen, Y. Yin, B. Chiaro, J. Mutus, C. Neill, P. O'Malley, P. Roushan, J. Wenner, T. C. White, A. N. Cleland, and J. M. Martinis, Coherent Josephson qubit suitable for scalable quantum integrated circuits, *Physical Review Letters* **111**, 080502 (2013).

<sup>193</sup> [13] Y. Chen, C. Neill, P. Roushan, N. Leung, M. Fang, R. Barends, J. Kelly, B. Campbell, Z. Chen, B. Chiaro, A. Dunsworth,

194 E. Jeffrey, A. Megrant, J. Y. Mutus, P. J. J. O’Malley, C. M. Quintana, D. Sank, A. Vainsencher, J. Wenner, T. C. White,  
 195 M. R. Geller, A. N. Cleland, and J. M. Martinis, Qubit architecture with high coherence and fast tunable coupling, Physical  
 196 Review Letters **113**, 220502 (2014).

197 [14] D. I. Schuster, A. Wallraff, A. Blais, L. Frunzio, R.-S. Huang, J. Majer, S. M. Girvin, and R. J. Schoelkopf, ac Stark shift  
 198 and dephasing of a superconducting qubit strongly coupled to a cavity field, Physical Review Letters **94**, 123602 (2005).

199 [15] A. Wallraff, D. I. Schuster, A. Blais, L. Frunzio, J. Majer, M. H. Devoret, S. M. Girvin, and R. J. Schoelkopf, Approaching  
 200 unit visibility for control of a superconducting qubit with dispersive readout, Physical Review Letters **95**, 060501 (2005).

201 [16] A. Blais, R.-S. Huang, A. Wallraff, S. M. Girvin, and R. J. Schoelkopf, Cavity quantum electrodynamics for superconducting  
 202 electrical circuits: An architecture for quantum computation, Physical Review A **69**, 062320 (2004).

203 [17] H.-S. Chang, Y. P. Zhong, K. J. Satzinger, M.-H. Chou, A. Bienfait, C. R. Conner, É. Dumur, J. Grebel, G. A. Pairs,  
 204 R. G. Povey, and A. N. Cleland, In preparation (2020).

205 [18] See supplementary material, which includes further information as well as Refs. [19-36], (2020).

206 [19] E. Jeffrey, D. Sank, J. Y. Mutus, T. C. White, J. Kelly, R. Barends, Y. Chen, Z. Chen, B. Chiaro, A. Dunsworth,  
 207 A. Megrant, P. J. J. O’Malley, C. Neill, P. Roushan, A. Vainsencher, J. Wenner, A. N. Cleland, and J. M. Martinis, Fast  
 208 accurate state measurement with superconducting qubits, Physical Review Letters **112**, 190504 (2014).

209 [20] J. Kelly, R. Barends, A. G. Fowler, A. Megrant, E. Jeffrey, T. C. White, D. Sank, J. Y. Mutus, B. Campbell, Y. Chen,  
 210 Z. Chen, B. Chiaro, A. Dunsworth, I.-C. Hoi, C. Neill, P. J. J. O’Malley, C. Quintana, P. Roushan, A. Vainsencher,  
 211 J. Wenner, A. N. Cleland, and J. M. Martinis, State preservation by repetitive error detection in a superconducting  
 212 quantum circuit, Nature **519**, 66 (2015).

213 [21] C. Macklin, K. O’Brien, D. Hover, M. E. Schwartz, V. Bolkhovsky, X. Zhang, W. D. Oliver, and I. Siddiqi, A near-  
 214 quantum-limited Josephson traveling-wave parametric amplifier, Science **350**, 307 (2015).

215 [22] D. M. Pozar, *Microwave Engineering*, 4th ed. (Wiley, Hoboken, NJ, 2012).

216 [23] J. M. Chow, L. DiCarlo, J. M. Gambetta, A. Nunnenkamp, L. S. Bishop, L. Frunzio, M. H. Devoret, S. M. Girvin, and  
 217 R. J. Schoelkopf, Detecting highly entangled states with a joint qubit readout, Physical Review A **81**, 062325 (2010).

218 [24] H. K. Xu, C. Song, W. Y. Liu, G. M. Xue, F. F. Su, H. Deng, Y. Tian, D. N. Zheng, S. Han, Y. P. Zhong, H. Wang, Y.-x. Liu,  
 219 and S. P. Zhao, Coherent population transfer between uncoupled or weakly coupled states in ladder-type superconducting  
 220 qutrits, Nature Communications **7**, 11018 (2016).

221 [25] K. Bergmann, H. Theuer, and B. W. Shore, Coherent population transfer among quantum states of atoms and molecules,  
 222 Reviews of Modern Physics **70**, 1003 (1998).

223 [26] B. W. Shore, *Manipulating Quantum Structures Using Laser Pulses* (Cambridge University Press, Cambridge, UK ; New  
 224 York, 2011).

225 [27] M. O. Scully and M. S. Zubairy, *Quantum Optics* (Cambridge University Press, Cambridge ; New York, 1997).

226 [28] G. S. Vasilev, A. Kuhn, and N. V. Vitanov, Optimum pulse shapes for stimulated Raman adiabatic passage, Physical  
 227 Review A **80**, 013417 (2009).

228 [29] S. Guerin, S. Thomas, and H. R. Jauslin, Optimization of population transfer by adiabatic passage, Physical Review A  
 229 **65**, 023409 (2002).

230 [30] T. Pellizzari, Quantum networking with optical fibers, Physical Review Letters **79**, 5242 (1997).

231 [31] B. Vogell, B. Vermersch, T. E. Northup, B. P. Lanyon, and C. A. Muschik, Deterministic quantum state transfer between  
 232 remote qubits in cavities, Quantum Science and Technology **2**, 045003 (2017).

233 [32] G. Lindblad, On the generators of quantum dynamical semigroups, Communications in Mathematical Physics **48**, 119  
 234 (1976).

235 [33] D. F. Walls and G. J. Milburn, *Quantum Optics*, 2nd ed. (Springer, Berlin, 2008).

236 [34] J. Johansson, P. Nation, and F. Nori, QuTiP: An open-source Python framework for the dynamics of open quantum

systems, Computer Physics Communications **183**, 1760 (2012).

[35] W. K. Wootters, Entanglement of formation of an arbitrary state of two qubits, Physical Review Letters **80**, 2245 (1998).

[36] M. B. Plenio and S. Virmani, An introduction to entanglement measures, arXiv:quant-ph/0504163 (2006), arXiv: quant-ph/0504163.

[37] Y.-D. Wang and A. A. Clerk, Using dark modes for high-fidelity optomechanical quantum state transfer, New Journal of Physics **14**, 105010 (2012).

[38] Y.-D. Wang, R. Zhang, X.-B. Yan, and S. Chesi, Optimization of STIRAP-based state transfer under dissipation, New Journal of Physics **19**, 093016 (2017).

[39] M. Neeley, M. Ansmann, R. C. Bialczak, M. Hofheinz, N. Katz, E. Lucero, A. O’Connell, H. Wang, A. N. Cleland, and J. M. Martinis, Process tomography of quantum memory in a Josephson-phase qubit coupled to a two-level state, Nature Physics **4**, 523 (2008).

[40] M. Steffen, M. Ansmann, R. C. Bialczak, N. Katz, E. Lucero, R. McDermott, M. Neeley, E. M. Weig, A. N. Cleland, and J. M. Martinis, Measurement of the entanglement of two superconducting qubits via state tomography, Science **313**, 1423 (2006).

[41] M. Neeley, R. C. Bialczak, M. Lenander, E. Lucero, M. Mariantoni, A. D. O’Connell, D. Sank, H. Wang, M. Weides, J. Wenner, Y. Yin, T. Yamamoto, A. N. Cleland, and J. M. Martinis, Generation of three-qubit entangled states using superconducting phase qubits, Nature **467**, 570 (2010).

[42] P. J. Mosley, J. S. Lundeen, B. J. Smith, P. Wasylczyk, A. B. U’Ren, C. Silberhorn, and I. A. Walmsley, Heralded generation of ultrafast single photons in pure quantum states, Physical Review Letters **100**, 133601 (2008).

[43] K. Azuma, K. Tamaki, and H.-K. Lo, All-photonic quantum repeaters, Nature Communications **6**, 6787 (2015).

[44] P. Kurpiers, M. Pechal, B. Royer, P. Magnard, T. Walter, J. Heinsoo, Y. Salathe, A. Akin, S. Storz, J.-C. Besse, S. Gasparinetti, A. Blais, and A. Wallraff, Quantum communication with time-bin encoded microwave photons, Physical Review Applied **12**, 044067 (2019).

[45] P. G. Kwiat, S. Barraza-Lopez, A. Stefanov, and N. Gisin, Experimental entanglement distillation and hidden non-locality, Nature **409**, 1014 (2001).

[46] R. Dong, M. Lassen, J. Heersink, C. Marquardt, R. Filip, G. Leuchs, and U. L. Andersen, Experimental entanglement distillation of mesoscopic quantum states, Nature Physics **4**, 919 (2008).

[47] H. Takahashi, J. S. Neergaard-Nielsen, M. Takeuchi, M. Takeoka, K. Hayasaka, A. Furusawa, and M. Sasaki, Entanglement distillation from Gaussian input states, Nature Photonics **4**, 178 (2010).

[48] J. F. Poyatos, J. I. Cirac, and P. Zoller, Quantum reservoir engineering with laser-cooled trapped ions, Physical Review Letters **77**, 4728 (1996).

[49] M. B. Plenio and S. F. Huelga, Entangled light from white noise, Physical Review Letters **88**, 197901 (2002).

[50] S. Hermelin, S. Takada, M. Yamamoto, S. Tarucha, A. D. Wieck, L. Saminadayar, C. Bauerle, and T. Meunier, Electrons surfing on a sound wave as a platform for quantum optics with flying electrons, Nature **477**, 435 (2011).

[51] R. P. G. McNeil, M. Kataoka, C. J. B. Ford, C. H. W. Barnes, D. Anderson, G. A. C. Jones, I. Farrer, and D. A. Ritchie, On-demand single-electron transfer between distant quantum dots, Nature **477**, 439 (2011).

[52] A. Baksic, H. Ribeiro, and A. A. Clerk, Speeding up adiabatic quantum state transfer by using dressed states, Physical Review Letters **116**, 230503 (2016).

[53] B. B. Zhou, A. Baksic, H. Ribeiro, C. G. Yale, F. J. Heremans, P. C. Jerger, A. Auer, G. Burkard, A. A. Clerk, and D. D. Awschalom, Accelerated quantum control using superadiabatic dynamics in a solid-state lambda system, Nature Physics **13**, 330 (2017).

[54] B. T. Torosov, S. Guerin, and N. V. Vitanov, High-fidelity adiabatic passage by composite sequences of chirped pulses, Physical Review Letters **106**, 233001 (2011).

280 [55] A. Bruns, G. T. Genov, M. Hain, N. V. Vitanov, and T. Halfmann, Experimental demonstration of composite stimulated  
281 Raman adiabatic passage, *Physical Review A* **98**, 053413 (2018).